Journal of Network Intelligence
Taiwan Ubiquitous Information
 ISSN 2414-8105 (Online)
Volume **7**, Number **4**, November **2022**

Remote Sensing Monitoring of Rice LAI Based on GRU-SVR

Chuhan Qi

School of Electronics Engineering
Heilongjiang University
No. 74 Xuefu Road, Harbin, China
qichuhan@aliyun.com

Xiaofei Wang*

School of Electronics Engineering
Heilongjiang University
No. 74 Xuefu Road, Harbin, China
nk_wxf@hlju.edu.cn

*Corresponding author: Xiaofei Wang

Received June 7, 2022, revised July 11, 2022, accepted September 9, 2022.

Abstract. *The rapid and accurate measurement of rice Leaf Area Index (LAI) is of great significance for evaluating rice growth and improving field management efficiency. Based on the PROSAIL model, this paper proposed a method to first extract characteristic bands using Two-Dimensional Correlation Spectrum (2DCOS), and then construct a GRU-SVR network to invert rice LAI. The experimental results show that the proposed method has higher inversion accuracy (R^2 = 0.92648, RMSE=0.63732), and is more suitable for the actual rice LAI inversion task. In addition, the generated LAI grading distribution map of rice within the study area makes it possible to master the growth situation of rice on a macro level, which could provide guidance and a broader perspective for subsequent field management.*
Keywords: Remote sensing; Rice leaf area index; Feature band extraction; Machine learning

1. **Introduction.** LAI can be expressed by the total leaf surface area of a plant population per unit land area [1]. It can not only participate in the estimation of terrestrial net ecosystem productivity [2], but also be used as an important parameter in the construction of various surface vegetation coverage monitoring models [3], environmental monitoring models [4] and hydrological models [5] as an important parameter. As an important parameter to characterize rice growth, LAI can provide dynamic information during the rice growth cycle, and its monitoring has important practical significance.

Sentinel-2 is a high-resolution multispectral imaging satellite launched by ESA [6]. The multi-spectrometer onboard can provide information every 5 days in 13 spectral bands ranging from visible to the short-wave infrared with a spatial resolution of up to 10 m across a width of 290 km. As a unique satellite with three bands of data in the red-edge band range, Sentinel-2 has outstanding advantages in monitoring land surface vegetation. Since its inception, the remote sensing data provided by Sentinel-2 has achieved fruitful results in forest monitoring [7], land cover change detection [8] and remote sensing mapping [9].

If there are too many training parameters in the neural network model, it will adversely affect the efficiency of the algorithm and the inversion accuracy. And the existing data redundancy and band autocorrelation in multispectral information will always lead to a waste of computing resources and difficulty in application in large-scale data sets [10], which is not suitable for practical applications. Therefore, it is necessary to screen out wavelengths specific for LAI to optimize the model. Qiao et al. [11]fused the morphological parameters extracted from the image information and spectral information with the vegetation index to construct a dynamic estimation model of maize LAI, and the experimental results proved that the model performed well in each growth period . Fukuda et al. [12]determined the extraction criteria of Simple ratio and NIR to PAR ratio through experiments, and successfully drew the dynamic curve of rice canopy growth season. Zhang et al. [13] screened feature bands highly correlated with winter wheat LAI from hyperspectral remote sensing image data and established a LAI estimation model based on extreme gradient lifting, proving that the accuracy of the LAI estimation model could be effectively improved by using feature bands with appropriate models.

At present, there are two main methods of LAI inversion: the empirical relation method and the physical model-based inversion method. The empirical relation method considers that LAI has a certain functional relation with the vegetation index calculated by the remote sensing surface reflectance, and LAI can be estimated by determining this relation. Dong et al. [14] selected 7 vegetation indices from the reflectance data of remote sensing images to estimate LAI of spring wheat and rapeseed, and found that the sensitivity of the VEGETATION indices established based on the reflectance of the visible band to LAI of different crops was better than other vegetation indices. Guo [15] used three kinds of multispectral image data to construct three vegetation indices for retrieving mangrove LAI, and proved the stability of retrieving mangrove LAI in different multispectral sensors by combining vegetation indices of visible and red-edge bands. However, the empirical relation method only uses several bands in the spectral range of remote sensing observation, which makes it difficult to achieve accurate fitting for LAI. The physical modeling method is a means to establish models of surface reflectance and LAI and other biophysical parameters observed by remote sensing based on the radiation transfer theory in vegetation canopy. Wan et al. [16] combined the PROSPECT model with spectral derivatives and similarity metrics to significantly improve the retrieval accuracy of leaf biochemical characteristics. Ren et al. [17] used LIBERTY model to generate simulated spectra, and further verified the ability of red-edge parameters and spectral index to detect soil moisture of winter wheat. The physical model has many parameters. Once the model is complicated, it will lead to various unpredictable problems in the inversion task. Therefore, it is necessary to set the parameters involved reasonably. The current hot research direction is to combine physical models with machine learning. Tian et al. [18] constructed a deep learning framework for yield estimation of winter wheat by using meteorological data, vegetation temperature index and LAI in the main growth periods of winter wheat, and the model accuracy was higher than that of the classical genetic algorithm. Li et al. [19]developed a Deep Neural Networks (DNN) model to estimate seasonal dynamic changes of corn LAI, proving that DNN can effectively deal with nonlinear problems and alleviate saturation spectrum. Machine learning has ushered in a bright future with the advantages of making it possible to manage high-dimensional data and map complex features [20].

The purpose of this study is to develop a practical, efficient and convenient inversion method of rice LAI, so as to realize macroscopic monitoring of rice growth and provide a broader perspective for field management. The main contributions of this paper are as follows:

(1) Use the PROSAIL model to generate simulated spectral data of rice canopy to increase the abundance of data set, improve model stability and avoid overfitting.

(2) After analyzing the disadvantages of the traditional feature band screening method, the 2DCOS method is used to screen the feature bands, which reduces the computational intensity while maintaining high accuracy.

(3) A rice LAI inversion model based on GRU-SVR is proposed. It combines SVR's ability to process small samples and nonlinear mapping with GRU's ability to run efficiently and deal with time series data. The model accuracy is fine-tuned using 70% of the measured historical data, making the model more suitable for the actual rice LAI inversion task in the field.

(4) The LAI distribution map is generated, which makes it possible to master the growth situation of crop groups from a macroscopic level, and provides technical support and guidance for subsequent field management.

2. Data acquisition and processing.

2.1. Spectral reflectance of rice canopy.

Figure 1 shows the curve of rice canopy spectral reflectance changing with LAI.It can be seen from Figure 1 that the canopy reflectance curve changes dynamically due to the disturbance of LAI: in the visible light range, the reflectance amplitude is inversely proportional to LAI; in the range of near-infrared to short-wave infrared, the reflectance amplitude is directly proportional to LAI, but the reflectance decreases or increases gradually with LAI changes. This variation is the theoretical basis for the inversion of rice LAI based on spectral data [21]. In addition, it can be found that the spectral reflectance of the rice canopy does not keep a linear change with the change of LAI, so it is difficult for the VEGETATION index constructed with less band reflectance to fully and accurately represent LAI, especially when LAI gradually increases, this method will lead to the underestimate of LAI.

2.2. Sentinel-2 remote sensing data.

Download the Sentinel-2 remote sensing image data on July 25, 2017 from the ESA official website. Sentinel-2 remote sensing images officially released by ESA are only finely geometrically corrected. Therefore, in order to obtain accurate remote sensing data, it is necessary to perform atmospheric correction and resampling on the obtained remote sensing images. In addition, the geographical location of the study area is $45°51' - 45°52'N, 126°47' - 126°48'E$, with a total of 404.594 acres, and the spatial resolution of the image after resampling is 10 m. Therefore, the size of the study area on the remote sensing image is 128×128. In order to highlight the research scope, the preprocessed remote sensing images were cropped into a region of 128×128 pixel size. The results of preprocessing satellite remote sensing images are shown in Figure 2.

2.3. PROSAIL simulation data.

The historical measured data set was collected from July to October 2017. Since the abundance of the measured dataset is not enough to fully mine all the information contained in the rice canopy spectrum, the PROSAIL model is used to generate a rice simulated canopy spectrum data set with LAI as the external perturbation for feature band selection, so as to explore as much information contained in the canopy spectral reflectance as possible. Table 1 shows the setting of rice biophysical quantity parameters involved in the PROSAIL model. Since there was no case of high chlorophyll concentration but small LAI, after excluding this part of the data, the simulated rice canopy spectral curve was generated based on a random combination of different parameters.

3. Rice LAI inversion based on GRU-SVR network.

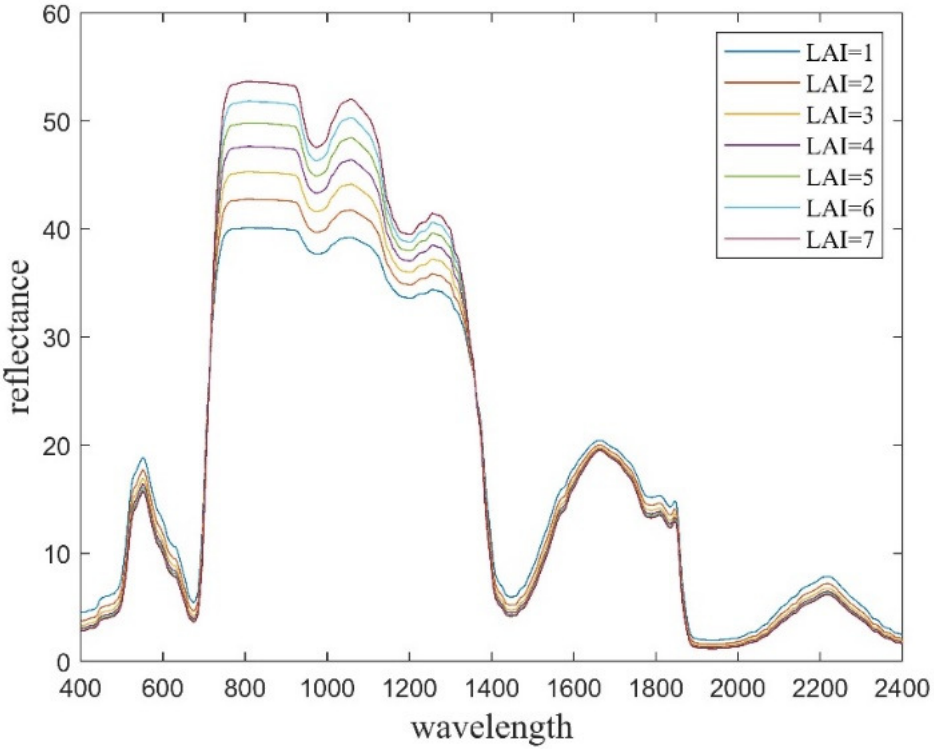

FIGURE 1. Curve of rice canopy reflectance changing with LAI

FIGURE 2. Results of sentinel-2 remote sensing image preprocessing

3.1. **DCOS.** Due to the wavelength limitation covered by the Sentinel-2 multi-spectrometer for vegetation observation, and the visible and near-infrared regions contain almost all feature bands related to crop photosynthetic pigments, spectral data in the range of 400-1000 nm was used for analysis. 2DCOS was used to extract the feature bands of the PROSAIL simulated canopy spectral data to obtain the combination of feature bands that could best characterize the rice LAI.

The change of a system caused by external perturbation can be manifested in the change of the spectrum, and the spectrum of this change is called dynamic spectrum. 2DCOS is

Table 1. PROSAIL blade optical characteristics parameters

Parameter	Range	Step length	Unit
Structural parameters of mesophyll	1.0-2.0	0.05	-
Chlorophyll content	20-80	10	$\mu g/cm^2$
Water content	0.02	-	cm
Dry weight	0.002-0.03	0.004	g/cm^2
Carotene content	8	8	$\mu g/cm^2$
Incident Angle	59	-	$^\circ$
LAI	0.1-8	0.01	-

to analyze the correlation between the two spectral signal intensity changes to obtain the spectral correlation intensities, and then expand them in the form of contour lines on a two-dimensional scale to study their dynamic spectrum [22].

Suppose there is a set of discretely-sampled spectra $A(\nu_j, \tau_k)$, where the spectral variable $\nu_j (j = 1, 2, ..., n)$ is measured under an external perturbation represented by the disturbance variable $\tau_k (k = 1, 2, ..., m)$. The spectral variable v can be wave number, frequency, wavelength, etc., and the external perturbation τ can be temperature, time, concentration, etc [23]. The continuous interval between τ_1 and τ_m defines the so-called observation interval of A. The average spectrum $\overline{A}(\nu_j)$ is defined as the reference spectrum of the system, and its expression is shown in Eq. (1). Then within$[\tau_1, \tau_k]$ interval, the dynamic spectral matrix $\overline{A}(\nu_j, \tau_k)$ of the system can be expressed by Eq. (2).

$$\overline{A}(\nu_j) = \frac{1}{m} \sum_{i=1}^{m} A(\nu_j, \tau_m) \tag{1}$$

$$\widetilde{A}(\nu_j, \tau_k) = A(\nu_j, \tau_k) - \overline{A}(\nu_j) \tag{2}$$

In 2DCOS, the correlation analysis of the intensity changes of two independent spectral variables (v1 and v2) resulting from the external perturbation is carried out, and the spectral correlation intensity $X(\nu_1, \nu_2)$ is obtained, as shown in Eq. (3):

$$X(\nu_1, \nu_2) = \phi(\nu_1, \nu_2) - i\psi(\nu_1, \nu_2) \tag{3}$$

In Eq. 3, $\phi(\nu_1, \nu_2)$ represents the intensity of synchronous correlation between two variables, and $\psi(\nu_1, \nu_2)$ represents the intensity of asynchronous correlation between two variables. For the generated simulated spectral data set can be expressed as dynamic spectrum $\widetilde{A}$ of $m \times n$, and its matrix element is defined as $\widetilde{A}(i, j) = \widetilde{A}(\nu_j, \tau_i)$, then $\phi(\nu_1, \nu_2)$ can be expressed as:

$$\phi(\nu_1, \nu_2) = \frac{1}{m-1} \widetilde{A}^T \widetilde{A} \tag{4}$$

As shown in Figure 3, the intensity of synchronization correlation is expanded in the form of contour lines in the two-dimensional coordinate system to obtain the synchronization correlation spectrum. The peaks obtained by the autocorrelation of dynamic spectral intensity changes on the sub-diagonal in the figure are called autocorrelation

peak. Its magnitude represents the extent to which the dynamic spectral correlation intensity changes under external perturbation conditions. Peaks symmetrical about the sub-diagonals are called synchronized cross peaks, which represent the consistency of intensity changes of two spectral signals (ν_1, ν_2) [24]. In any region of the dynamic spectrum, when the spectral intensity changes significantly due to external perturbation, there will be strong autocorrelation peaks. Therefore, the autocorrelation peak can be used as an important basis for selecting the feature band. The peak intensity represents the sensitivity of spectral signal intensity to external perturbation, and the coordinate of the peak represents the position of the feature band.

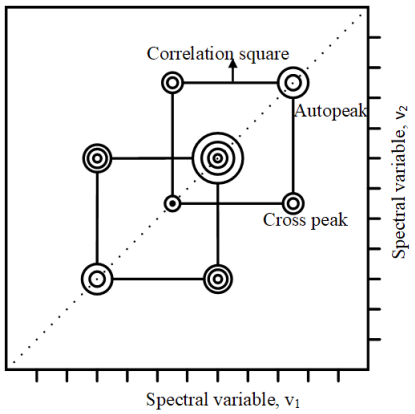

FIGURE 3. Synchronous correlation spectrum

In this paper, the rice LAI was considered as an external perturbation that affects the spectral reflectance of rice canopy. As LAI changes, the corresponding change spectrum can be regarded as dynamic spectrum. The externally perturbed LAI values generated by the PROSAIL model were uniformly distributed, meeting the use conditions of 2DCOS. Perform 2DCOS on the simulated spectral data obtained from PROSAIL, observe the changes of synchronous correlation spectral intensity under the disturbance of LAI, and extract feature bands, as shown in Figure 4.

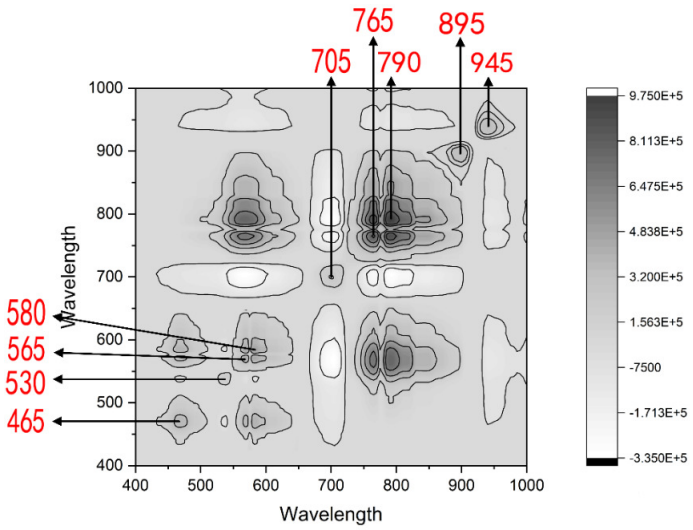

FIGURE 4. Positions of feature bands in synchronous correlation spectrum

It can be seen from Figure 4 that there are 9 autocorrelation peaks located at 465, 530, 565, 580, 705, 765, 790, 895, and 945 nm respectively. The spectral correlation intensities located around these bands are highly sensitive to external perturbation, so they show good correlation with LAI in aspects of photosynthesis mechanism, molecular structure and optical properties, and can be used as feature bands to invert rice LAI.

Comparing the feature bands screened by the 2DCOS method with SMLR, the result is shown in Figure 5. It can be seen that the positions of some feature bands selected by the two methods coincide, such as band 530, 765 and 945 nm. However, the bands selected by the SMLR method have regional aggregation, with dense distribution in some band ranges and sparse distribution in some band ranges. As a result, the feature bands are unevenly distributed in the entire spectral research range, which is not conducive to fully excavating the information contained in the rice canopy spectrum, nor to fully utilizing the remote sensing data provided by the Sentinel-2 multi-spectrometer. In addition, within the range of near-infrared bands that Sentinel-2 satellite can observe, SMLR method does not select feature bands, which are sensitive to LAI, chlorophyll content and crop biomass. Therefore, feature bands not included in this range are not rigorous for inversion of crop LAI. 2DCOS selected a band of 895 nm, fully excavated the feature bands sensitive to rice LAI, and provided sufficient characteristic information for subsequent research. Therefore, the feature bands selected by 2DCOS have stronger LAI representativeness and pertinence.

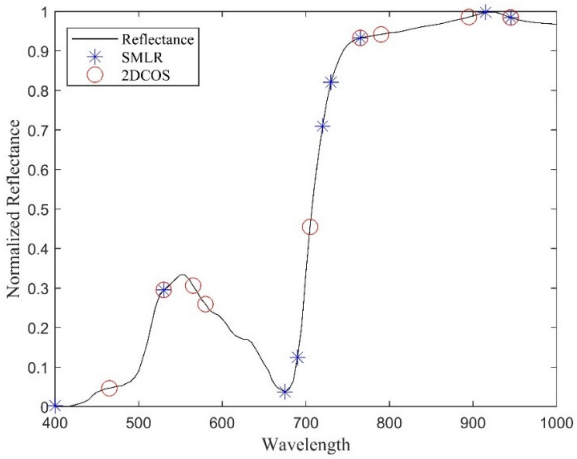

FIGURE 5. Position comparison of feature bands

SMLR method analyzes the significance of each feature band introduced into the model, and finally selects the most significant feature band set, and the model established based on this set has high accuracy. Therefore, using the SMLR method as a control can better illustrate the advantages of the 2DCOS method. Compared with SMLR method for significance analysis of each feature band, the underlying logic of the 2DCOS method for screening feature bands is to analyze the correlation of intensity changes of spectral variables with external perturbation, so all feature bands with specificity for LAI of rice can be screened without omitted. In addition, the 2DCOS method can intuitively display the position of feature bands and the sensitivity of spectral reflectance to changes in external perturbation, and it takes much less time than SMLR method. Therefore, the feature bands screened by 2DCOS method can accurately characterize the rice LAI and maintain high accuracy while reducing the amount of calculation.

3.2. **GRU network.** Although the experiments in [25] show that SVR has higher regression analysis ability than LSTM [26], the SVR algorithm cannot make full use of the timing sequence of rice LAI data, and the algorithm has many parameters, so its operation efficiency is not high when processing a large number of sample data. RNN network can discover the temporal sequence characteristics of rice LAI and make use of it, but the number of samples required is large, which is difficult to obtain in general, and the robustness is not strong. Therefore, combining the advantages of the two algorithms, a rice LAI inversion model based on GRU-SVR was proposed and constructed.

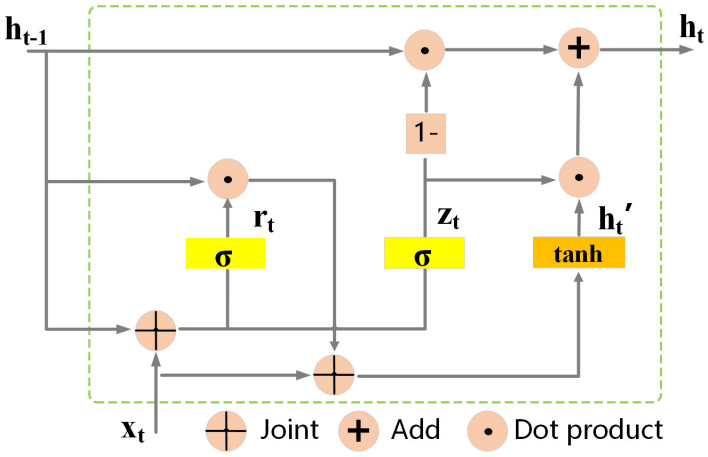

FIGURE 6. GRU hidden unit structure diagram

GRU performs certain deformation optimization on the internal structure of the hidden unit of LSTM [27], which is becoming more and more popular due to its advantages of efficiency and simplicity. As shown in Figure 6, each hidden unit of GRU contains two gating units, reset gate and update gate, to realize the selective memory of information. Compared with other deformation structures of RNN, it uses fewer parameters, greatly reduces the amount of calculation, and can achieve the same level of accuracy, which is suitable for tasks requiring multiple experiments.

(1)Reset gate(r_t)

The reset gate is used to determine the extent to which the previous hidden unit state h_{t-1} can be updated to the current temporary hidden unit state h'_t. When the signal is obtained, h_{t-1} obtains the reset data through the dot product operation with r_t , and then integrates the data with the current input x_t, and the obtained result compress the output h'_t compressed between $(-1, 1)$ through the tanh function. The process is shown in Eqs. 5 and 6.

$$r_t = \sigma(W_r x_t + U_r h_{t-1} + b_r) \tag{5}$$

$$h'_t = tanh(W_h x_t + U_h(r_t \cdot t - 1) + b_n) \tag{6}$$

When r_t is 0 or close to 0, h_{t-1} does not participate in the calculation, and all information sources of h'_t are x_t , that is, h_{t-1} is reset. When r_t is 1 or close to 1, the information sources of h'_t are x_t and h_{t-1}.

(2) Update gate(z_t)

The update gate is used to determine how much h_{t-1}) can update to the current hidden unit state h_t , and how much information on h_t needs to accept from the candidate state

h'_t . When the signal is obtained, first forget the unnecessary information in h_{t-1} through the dot product operation of h'_{t-1} and $(1 - z_t)$ (Eq. 7), and then the information needed in h'_t is remembered through the dot product operation of h'_t and z_t (Eq.8).

$$z_t = \sigma(W_z x_t + U_z h_{t-1} + b_z) \tag{7}$$

$$h_t = z_t \cdot h_{t-1} + (1 - z_t) \cdot h'_t \tag{8}$$

Since z_t is derived from σ function, its value range is $(0, 1)$, and the closer its value is to 1, the more data is left. According to Eq. 8, the more previous data is left, the less current data is added. h'_t and h_{t-1} are in a state of competition. Eqs. 5 to 8 constitute the GRU forward propagation formula.

3.3. **Model construction.** The matlab2019b software was used to build the rice LAI inversion model based on GRU-SVR, and the model architecture is shown in Figure 7. The data set is composed of the simulated spectral reflectance data and LAI values corresponding to the feature bands selected by the 2DCOS method.

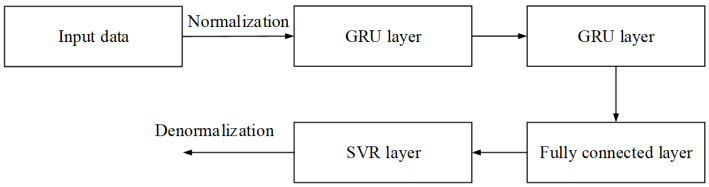

FIGURE 7. GRU-SVR inversion model structure

The final output layer of the GRU network is the softmax function and SVR is taken as the final output layer of GRU network to realize the combination of the GRU network and the SVR algorithm (Figure 7). The data processing process of the model is: firstly, normalize the data set, and initialize the parameters of the GRU layer and the SVR layer. Secondly, use the preprocessed data to train the GRU layer. A total of two GRU layers are set up, each layer randomly disconnects 30% of units, and the output data of the second GRU layer is defined as 'sequence'. Then the output of the second GRU layer is sent to the SVR layer as input to continue training. Finally, the output of the SVR layer is denormalized and the result is displayed. The generalization and regression effects of the model are directly affected by the selection of its parameters [28]. After a lot of experiments, the optimal values of the parameters of the model are finally determined. The input sequence dimension is the number of feature bands. Different numbers of hidden nodes are set in the two GRU layers. A total of 300 epochs of training were set, and the initial learning rate was specified as 0.005. After the 130th epoch of training, the learning rate was reduced by multiplying by a factor of 0.18. The parameters of the SVR layer are shown in Table 2.

4. Experimental results and analysis.

4.1. **Kernel function selection.** The data set was constructed using PROSAIL simulation data. The attribute matrix of the data set was constructed by the spectral reflectance corresponding to each feature band, and the data set was labeled as the corresponding LAI value. Based on different kernel functions, SVR-based rice LAI inversion models were constructed. Randomly select 100 sample points and 100 corresponding inversion values to generate scatter plot and error bar plot. According to these two images, the performance of the model can be visually observed.

TABLE 2. Parameters of the SVR layer

Symbol	Role	Default value
s	Set SVM type	0, 1, 2, 3, 4
t	Set the kernel function type	0, 1, 2, 3
d	Set the degree of the kernel function	3
g	Set the gama of the kernel function	$1/t$
r	Set the coef0 of the kernel function	0
c	set penalty factor	1
ν	Set up cross-validation	≥ 2

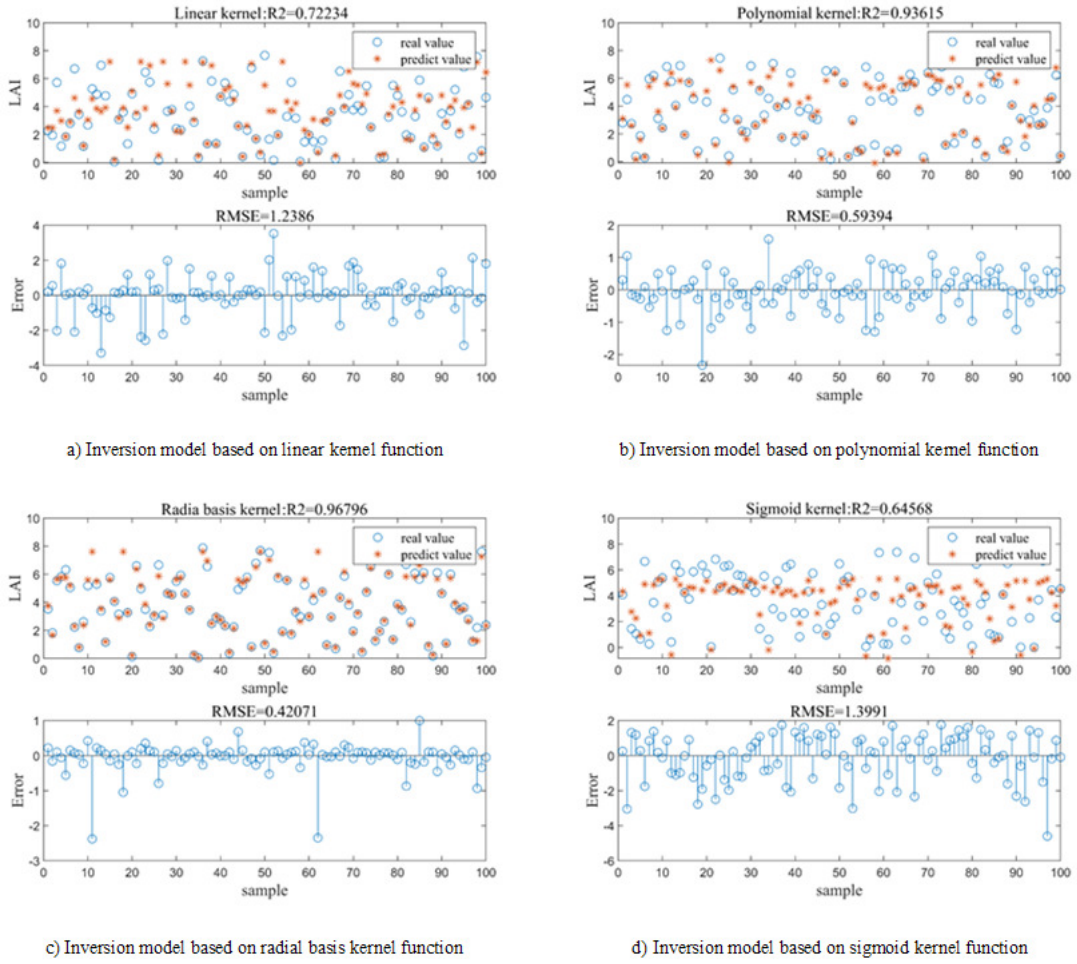

FIGURE 8. Inversion models based on different kernel functions

It can be seen from Figure 8 that the fitting degree of the model based on the linear kernel function reaches 0.72234, which can support the model to complete the rough accuracy inversion of LAI, but cannot meet the requirements of precision agriculture. This is because the linear kernel function is not strong enough to deal with nonlinear problems. The accuracy of the inversion model based on the polynomial kernel function is generally higher than that based on the linear kernel function: the fitting degree increases by about 20 percentage, and the error decreases by about 0.6. This is because the polynomial kernel is more suitable for solving nonlinear problems and the power series of the highest order

term can be set according to the need to improve the degree of fitting. Compared with the polynomial model, the accuracy of the model based on radial basis kernel function is improved but the scale is not too large. However, because the polynomial kernel function involves many parameters, the time consumed in the parameter optimization process increases greatly. And the polynomial kernel function is not suitable for the case of higher power. The performance of the model based on sigmoid kernel function is generally worse than that based on linear kernel function, because sigmoid kernel function is difficult to meet the requirements of SVR for matrix attributes of kernel function, and the function is derived from neural network, which is more suitable for solving classification problems.

Table 3. Accuracy of each model

Method name	Kernel type	R^2	RMSE
SMLR	Linear kernel	0.71358	1.2579
	Polynomial kernel	0.90707	0.71652
	Radial basis kernel	0.93866	0.58213
	Sigmoid kernel	0.62606	1.4373
2DCOS	Linear kernel	0.72234	1.2386
	Polynomial kernel	0.93615	0.59394
	Radial basis kernel	0.96796	0.42071
	Sigmoid kernel	0.64568	1.3991

It can be seen from Table 4-1, under the conditions of different selection methods of feature bands, the model established by 2DCOS method has higher accuracy. Among the inversion models constructed based on different kernel functions, the inversion model based on radial basis kernel function has the highest accuracy. These results first prove that the feature bands selected by the 2DCOS method are highly sensitive to LAI while eliminating redundancy. Secondly, LAI inversion model of rice should be established by using the radial basis kernel function.

4.2. **Rice LAI Inversion based on GRU-SVR network.** Radial basis kernel function was used to construct SVR layer, and data sets were constructed according to the feature bands screened by 2DCOS. The performance of the proposed model is shown in Figure 9.

Based on Table 3 and Figure 9, it can be seen that the proposed model combines the advantages of GRU network, which is efficient and can process time series data, with the advantages of SVR, which is stable and can carry out nonlinear mapping. Satisfactory results had been achieved in terms of fitting degree and error control.

4.3. **Add historical measured data to fine-tune model accuracy.** Because the debugging environment of the previously established model is simulation environment, the performance of the model will be greatly reduced if it is directly applied to the practical tasks. Therefore, historically measured data is added to the simulated data set and the model is retrained. The historical measured data were collected from July to October in 2017, and the geographic location of the collection area was $45°51' - 45°52'N, 126°47' - 126°48'E$.

As shown in Figure 10, with the increase of the number of historically measured samples, the model accuracy keeps increasing. When 50% of the historical measured data is added,

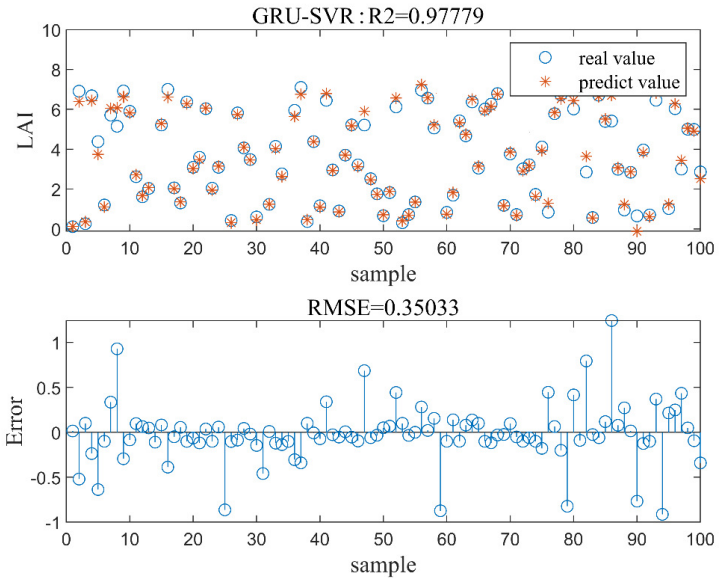

FIGURE 9. Accuracy of GRU-SVR inversion model

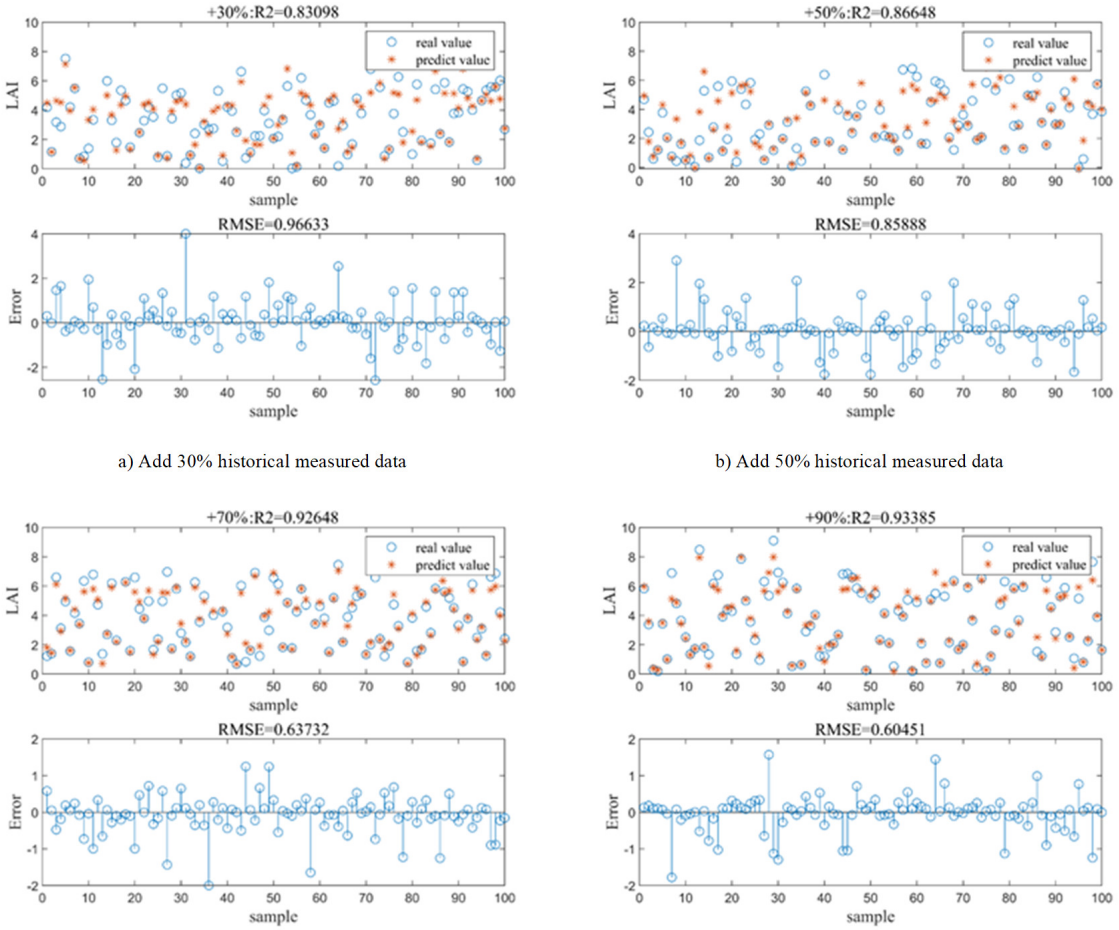

a) Add 30% historical measured data

b) Add 50% historical measured data

c) Add 70% historical measured data

d) Add 90% historical measured data

FIGURE 10. Fine-tuning the accuracy of the inversion model

the accuracy of the model is significantly improved compared with 30%, reaching an acceptable level. The historical measured data is further increased to 70%, and the accuracy of the model is greatly improved to a satisfactory and stable level. When it is increased to 90%, although the model accuracy is improved, the scale is not large and the model running time will be increased. Therefore, the feature band data screened out by 2DCOS method plus 70% historical measured sample data should be used.

Figure 11 shows the inversion accuracy of the three models. It can be seen that, compared with the single inversion model based on GRU network, the proposed model with SVR performs better: the fitting degree is improved and the error is greatly reduced. Compared with the single SVR based inversion model, the proposed model has a more obvious ability in improving the fitting degree and error control, which proves the importance of reasonable and sufficient temporal data characteristics. In general, the proposed GRU-SVR model inherits the advantages of two kinds of machine learning methods, and has outstanding advantages in the improvement of fitting degree and error control, which proves that the proposed model has certain practical significance in rice LAI inversion.

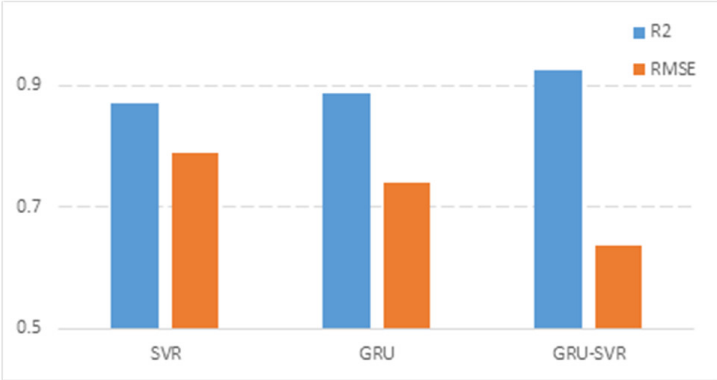

FIGURE 11. Fine-tuning the accuracy of the inversion model

4.4. **Remote sensing monitoring of rice LAI.** The preprocessed Sentinel-2 remote sensing image (Figure 2b) was applied to the trained model to obtain the LAI value of each pixel, and then output the LAI grading distribution map (Figure 12).

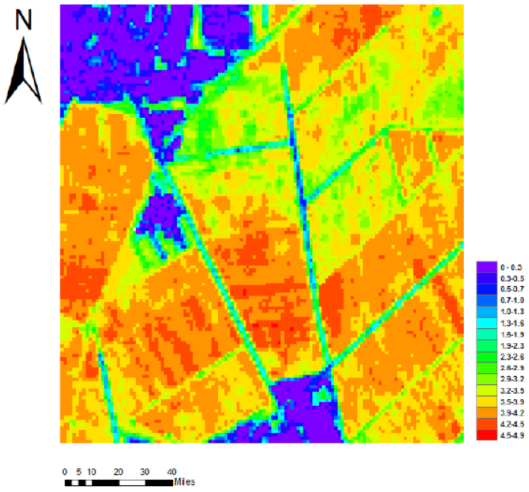

FIGURE 12. Fine-tuning the accuracy of the inversion model

The remote sensing image in Figure 12 was collected on July 25, 2017, when rice would pass jointing stage and enter the booting stage. During this time period, the LAI of rice increased continuously with plant growth. According to historical data and rice planting experience, the LAI of rice in this period should be between 3 and 5, and the LAI distribution in the figure is consistent with the actual situation. Therefore, it can be concluded that the rice growth in the study area was normal at this time. In addition, the observation of the image showed that the LAI values at the edge of the farmland were generally smaller than those inside the farmland, which may be due to the poor crop growth conditions due to the influence of the surrounding urban living areas. It may also be that there is no rice planting in these areas, so the model cannot use the spectral information screened for rice to fit LAI. In conclusion, it is feasible and effective to use the proposed model to monitor the growth status of rice on the remote sensing platform, and can provide guidance or reference for subsequent field management or yield estimation.

5. **Conclusions.** LAI is a key indicator that can directly reflect the growth of rice, and monitoring the dynamic changes of rice LAI is of great significance for promoting precision agriculture.

In this paper, a rice LAI inversion model based on GRU-SVR was constructed, and nine feature bands sensitive to rice LAI at 465, 530, 565, 580, 705, 765, 790, 895, and 945 nm were screened out by 2DCOS method. In order to improve the universality of the model, 70% of historical measured data was added to the simulation data set to construct the data set. The experimental results showed that compared with other models, the performance of the proposed model was the best (R2=0.92648, RMSE=0.63732). Finally, the LAI distribution map was obtained by applying Sentinel-2 remote sensing images to the trained model, and the results were consistent with the actual situation in the field, which proved that the proposed model has practical significance for the actual rice LAI inversion task in the field.

Future studies also need to consider how to screen out useful information related to rice crops from mixed information (such as soil, weeds, etc.) to improve the inversion accuracy. In addition, the development of spectrometers that are more cost-effective, simple, portable, and easy to operate is also an important direction.

Acknowledgment. This work is supported by National Natural Science Foundations of China (61871150), National Key R&D Program of China (2016YFB0502502).

REFERENCES

[1] G. G. Parker, "Tamm review: Leaf Area Index (LAI) is Both a Determinant and a Consequence of Important Processes in Vegetation Canopies," *Forest Ecology and Management*, vol. 477, 118496 ,2020

[2] S. Yang, L. Hu, H. Wu, H. Ren, W. Fan, "Integration of Crop Growth Model and Random Forest for Winter Wheat Yield Estimation From UAV Hyperspectral Imagery," *Journal of Selected Topics in Applied Earth Observations and Remote Sensing*, vol. 14, pp. 6253-6269, 2021

[3] Y. Hu, H. Li, D. Wu, W. Chen, M. Hou, A. Li, Y. Zhu, "LAI-Indicated Vegetation Dynamic in Ecologically Fragile Region: A Case Study in the Three-North Shelter Forest Program Region of China," *Ecological Indicators*, vol. 60,pp. 1-14, 2022

[4] X. Zhu, J. Li, Q. Liu, W. Yu, S. Lin, "Use of a BP Neural Network and Meteorological Data for Generating Spatiotemporally Continuous LAI Time Series," *Science of The Total Environment*, vol. 821,153180, 2022

[5] H. Haas, L. Kalin, P. Srivastava, "Improved Forest Dynamics Leads to Better Hydrological Predictions in Watershed Modeling," *Science of The Total Environment*, vol. 821, 153180, 2022

[6] T. Sun, Q. Qin, H. Ren, Y. Zhang, "Decameter Cropland LAI/FPAR Estimation From Sentinel-2 Imagery Using Google Earth Engine," *IEEE Transactions on Geoscience and Remote Sensing*, vol. 60,pp. 1-14, 2022

[7] J. Hemmerling, D. Pflugmacher, P. Hostert, "Mapping Temperate Forest Tree Species Using Dense Sentinel-2 Time Series," *Remote Sensing of Environment*, vol. 267, 112743, 2021

[8] K. Kowalski, A. Okujeni, M. Brell, P. Hostert, "Quantifying drought effects in Central European grasslands through regression-based unmixing of intra-annual Sentinel-2 time series," *Remote Sensing of Environment*, vol. 268,112781, 2022

[9] G. Maskell, A. Chemura, H. Nguyen, "Integration of Sentinel Optical and Radar Data for Mapping Smallholder Coffee Production Systems in Vietnam," *Remote Sensing of Environment*, vol. 266, 112709, 2021

[10] W. Sun, Q. Du, "Hyperspectral Band Selection: A Review, " *IEEE Geoscience and Remote Sensing Magazine*, vol. 7,no.2,pp. 118-139, 2019

[11] L. Qiao, D. Gao, R. Zhao, W. Tang, L. An, M. Li, H. Sun, "Improving estimation of LAI dynamic by fusion of morphological and vegetation indices based on UAV imagery," *Computers and Electronics in Agriculture*, vol. 192, 106603, 2022

[12] S. Fukuda, K. Koba, M. Okamura, Y. Watanabe, D. Sugiura, "Novel Technique for Non-destructive LAI Estimation by Continuous Measurement of NIR and PAR in Rice Canopy," *Field Crops Research*, vol. 263, 108070, 2021

[13] J. Zhang, T. Cheng, W. Guo, X. Xu,H. Qiao, "Leaf Area Index Estimation Model for UAV Image Hyperspectral Data Based on Wavelength Variable Selection and Machine Learning Methods," *Plant Methods*, vol. 17,no.1,49, 2021

[14] T. Dong, J Liu, J. Shang, B. Qian, B. Ma, K. John M,W. Dan, X. Jiao, X. Geng, Y. Shi, "Assessment of Red-Edge Vegetation Indices for Crop Leaf Area Index Estimation," *Remote Sensing of Environment*, vol. 222,pp.133-143, 2019

[15] X. Guo, M. Wang, M. Jia, W. Wang, "Estimating Mangrove Leaf Area Index Based on Red-Edge Vegetation Indices: A Comparison among UAV, WorldView-2 and Sentinel-2 Imagery," *International Journal of Applied Earth Observation and Geoinformation*, vol. 103, 102493, 2021

[16] L. Wan, J. Zhang, Y. Xu, Y. Huang, W. Zhou, L. Jiang, Y. He, H. Cen, "PROSDM: Applicability of PROSPECT Model Coupled with Spectral Serivatives and Similarity Metrics to Retrieve Leaf Biochemical Traits from Bidirectional Reflectance," *Remote Sensing of Environment*, vol. 267,no.15, 112761, 2021

[17] S. Ren, B. Guo, Z. Wang, J. Wang, Q. Fang, J. Wang, "Optimized Spectral Index Models for Accurately Retrieving Soil Moisture (SM) of Winter Wheat Under Water Stress," *Agricultural Water Management*, vol. 261,no.1, 107333, 2022

[18] H. Tian, P. Wang, K. Tansey, D. Han, J. Zhang, S. Zhang, H. Li, "A Deep Learning Framework under Attention Mechanism for Wheat Yield Estimation Using Remotely Sensed Indices in the Guanzhong Plain," *PR China, International Journal of Applied Earth Observations and Geoinformation*, vol. 102, 102375, 2021

[19] Y. Li, Y. Ren, W. Gao, J. Jia, S. Tao, X. Liu, "An Enhanced Spatiotemporal Fusion Method - Implications for DNN Based Time-Series LAI Estimation by Using Sentinel-2 and MODIS," *Field Crops Research*, vol. 279,108452, 2022

[20] P. M. Atkinson, A. Stein, C. Jeganathan, "Spatial Sampling, Data Models, Spatial Scale and Ontologies: Interpreting Spatial Statistics and Machine Learning Applied to Satellite Optical Remote Sensing," *Spatial Statistics*, vol. 100646, 2022

[21] S. Liu, W. Zeng, L. Wu, G. Lei, B. Zhou, J. Huang, "Simulating the Leaf Area Index of Rice from Multispectral Images," *Remote Sensing*, vol. 13,no.18, 3663, 2021

[22] J. Yue, Z. Li, Z. Zuo, Y. Zhao, J. Zhang, Y. Wang, "Study on the Identification and Evaluation of Growth Years for Paris Polyphylla var. yunnanensis Using Deep Learning Combined with 2DCOS," *Spectrochimica Acta Part A: Molecular and Biomolecular Spectroscopy*, vol. 261, 120033, 2021

[23] I. Noda, "Recent Advancement in the Field of Two-Dimensional Correlation Spectroscopy," *Journal of Molecular Structure*, vol. 883/884,pp.2-26, 2007

[24] I. Noda, "Vibrational two-dimensional correlation spectroscopy (2DCOS) study of proteins," *Spectrochimica Acta Part A: Molecular and Biomolecular Spectroscopy*, vol. 187,pp.119-129, 2017

[25] M. Wu, J. Syu, C. Chen, "Kelly-based options trading strategies on settlement date via supervised learning algorithms," *Computational Economics*, vol. 59,no.4,pp. 1627-1644, 2022

[26] S. Kumar, A. Damaraju, A. Kumar, S. Kumar, C. Chen, "LSTM Network for Transportation Mode Detection," *Journal of Internet Technology*, vol. 22,no.4,pp. 891-902, 2021

[27] E. Wang, X. Zhang, F. Wang, T. Wu, C. Chen, "Multilayer dense attention model for image caption," *IEEE Access*, vol. 7,pp. 66358-66368, 2019

[28] L. Kang, R. Chen, N. Xiong, Y. chen, C. Chen, Y. Hu, C. Chen, "Selecting Hyper-Parameters of Gaussian Process Regression Based on Non- Inertial Particle Swarm Optimization in Internet of Things," *IEEE Access*, vol. 7,pp.59504-59513, 2019